Hindawi
Geofluids
Volume 2021, Article ID 8848932, 10 pages
https://doi.org/10.1155/2021/8848932

Research Article

Evaluation of Coal Pore Connectivity Using N_2 Sorption Isotherm and Spontaneous Imbibition Tests

Tong-qiang Xia,[1,2,3] **Jiao-fei He**,[3] **Shi-xing Fan**,[2] **Qiang-qiang Zhang**,[3] **Zi-long Li**,[2,3] **and Dun-shuai Sun**[3]

[1]*Shaanxi Provincial Key Laboratory of Geological Support for Coal Green Exploitation, Xi'an University of Science and Technology, Xi'an 710054, China*
[2]*State Key Laboratory of Coal Resources in Western China, Xi'an University of Science and Technology, Xi'an 710054, China*
[3]*School of Electrical and Power Engineering, China University of Mining and Technology, Xuzhou 221008, China*

Correspondence should be addressed to Tong-qiang Xia; tq.xia@cumt.edu.cn and Zi-long Li; ts20130011a31@cumt.edu.cn

Received 25 August 2020; Revised 14 June 2021; Accepted 15 July 2021; Published 19 August 2021

Academic Editor: Guanglong Sheng

Pore structure and connectivity of coal are critical factors in coal gas migration and production, which can be characterized by studying the kinetics of capillary imbibition behaviour within the pore spaces. In order to investigate them, six typical coal samples from different collieries in China (Yangcun, Changcun, Gengcun, Yanbei, Dongxia, and Yuwu coal) are selected to carry out N_2 sorption isotherm and spontaneous imbibition tests. Results from N_2 sorption isotherm tests show that there is a great difference between the total specific surface area and total pore volume among the six coal samples. Their total specific surface area varies from 0.302 to 3.275 m^2/g, and the total pore volume varies from 1.782 to 10.94 mm^3/g. The pore volume relationship of coal sample among them is in order from the large to small: Dongxia>Yangcun>Gengcun>Yuwu>Changcun>Yanbei coal, and the specific surface area is in order from the large to small: Yangcun>Dongxia>Changcun>Yuwu>Gengcun>Yanbei coal. The imbibition characters of six coal samples were matched using explicit the short-time limit ($t \longrightarrow 0$) and long-time limit ($t \longrightarrow \infty$) models by Zhmud et al., respectively. The results show that the long-time limit ($t \longrightarrow \infty$) model is better. Combined with pore structure analysis, it can be qualitatively analyzed that the imbibition capacity of six coal samples is positively correlated with the connectivity of coal pores, which is ranked as Changcun>Yanbei>Gengcun>Yangcun>Dongxia>Yuwu coal. This work will help understand the mechanism controlling fluid loss and ultimate gas/oil recovery in unconventional hydrocarbon exploration.

1. Introduction

Coal seam gas has long been considered a promising future source of energy worldwide [1, 2]. The coal seam permeability in most Chinese mines (except the southern Qinshui coalfields) ranges between $10^{-4} \sim 10^{-3}$ mD, which is four and three orders of magnitude lower than those in the U.S. and Australia, respectively [3, 4]. Given concerns regarding the efficient exploration of coal gas, horizontal drilling and hydraulic fracturing have played an increasingly important role in coal gas development over the past several decades [5, 6]. During the hydraulic fracturing process, huge water loss will take place because of the injected high-pressure water and capillary imbibition of water [7, 8]. Water imbibition of coal is defined for a water phase displaces a gas phase by capillary force only [9]. It may occupy the fracture passage and block the migration and diffusion of coal gas. In addition, the moisture content of the coal matrix also has an important influence on the gas adsorption characteristics. Over the past few years, despite having success in gas production from coal reservoirs in China, many technical questions associated with petrophysical properties of coals and fracturing fluid loss induced water lock phenomenon remain unanswered [10, 11]. Capillary imbibition of water is an important mechanism controlling the water loss and ultimate gas recovery [12, 13]. It probably has a significant influence on the increase of initial gas production rate after a long shut-in period, as the effective imbibition of fracturing water into

coal matrix [14, 15]. Consequently, for better understanding the migration and accumulation of coal gas, it is essential to investigate the imbibition characteristics of coal under the exploitation process using hydraulic fracturing.

The capillary imbibition process of water in coal involves a series of fluid-coal interactions, including coal particles swelling, mineral dissolution, and water adsorption, which could alter the pore structure of coal and then affect the gas recovery process [16]. To obtain a better understanding of the capillary imbibition process in the porous media, there are many publications associated with its mathematical description and its physical explanation to deal with this problem. For example, Green and Ampt [17] developed a theoretical model of the capillary rise in a thin tube based on Poiseuille's law. Lucas [18] and Washburn [19] neglected the inertia effect and further developed this theory independently to gain the relation between the capillary rise and time as ignorance of the gravitational and kinetic effects. Masoodi et al. [20] derived a capillary rise model in a vertical tube with consideration of the kinetic, gravity, and viscous effects. Fries and Dreyer [21] proposed an analytical solution for the capillary rise of liquid in a cylindrical tube. John and Tarik presented an experimental and numerical study of capillary imbibition in tubes while undergoing a phase change. Mohammad and Bassam studied the capillary rise in vertical tubes using fluid in rigid-body motion approach by transforming the nonlinear Lucas–Washburn equation to a linear mass-spring-damper system [22]. Roychaudhuri et al. thought fluid loss during hydraulic fracturing could be explained at least partly by imbibition processes, based on imbibition water experiments of shale samples [23]. Dehghanpour et al. attributed the water intake excess to water adsorption by clay minerals and adsorption-induced microfractures by investigating the imbibition of deionized water in gas shales [24]. Gao and Hu correlated the derived wettability to pore structure and mineralogy of shale samples using the directional imbibition experiments [25]. Subsequently, they investigated the effects of initial water saturation and imbibing fluid on the imbibition water process [26]. Wu et al. studied the influence of water imbibition on gas desorption in coal and found that water can promote the displacement desorption of adsorbed gas in coal, and the larger the water content is, the greater the displacement desorption amount is [27]. Compared with other oil/gas shale rocks, coal is more prone to expansion, dissolution, and softening by imbibition water. An increasing number of studies have recently been focused on the imbibition characteristics of shale or rock samples. However, given the complexity of the process of coal imbibition water, few imbibition water experiments of coal were conducted out [28]. This knowledge gap defines the purpose of our study.

In this work, our aim was to study the pore connectivity of coal and to further understand the gas migration and accumulation mechanism of these low permeability reservoirs of coal; it is not about the connectivity of coal seams for the multilevel area. The coal samples we selected come from different regions and different kinds of coal, and the coal samples have certain typicality. The coal samples would be selected to carry out N_2 sorption isotherm and spontaneous imbibition tests. N_2 adsorption method was conducted to obtain the pore size distribution and specific surface area of coal samples [29, 30]. Furtherly, water imbibition of coal samples was utilized to analyze the process that a wetting fluid displaces a nonwetting fluid in porous media by capillary forces. The results would help to further understand the gas migration and accumulation mechanism of these low permeability reservoirs of coal.

2. Samples and Methodologies

2.1. Samples. Six coal samples from different collieries including Yangcun, Changcun, Gengcun, Dongxia, and Yuwu collieries were collected for analyses of pore construction characteristics and capillary imbibition phenomena. When we selected coal samples to carry out the laboratory, we chose 2-3 pieces for a set of coal samples to ensure the reproducibility of the experiment. We could not guarantee that the pore-crack system of coal samples was completely homogeneous. In the production process of coal samples, we as much as possible ensured that the structure of coal samples would not be damaged with the minimum disturbance. The location of coal samples was shown in Figure 1.

2.2. Methodologies

2.2.1. PSD Determined by Low-Pressure Nitrogen Adsorption. N_2 adsorption method has been widely applied to evaluate the pore volume and pore size distribution (PSD) of coal samples. The coal samples of the above six coal mines were crushed to 60–80 mesh sizing and dried at 110°C for at least 12 h to remove adsorbed moisture and capillary water. A serial of N_2 ad-desorption isotherm experiments was conducted under the relative pressures (p/p_0) of standard liquid N_2 ranging from 0.01 to 1 at the Autosorb iQ automatic gas adsorption analyzer of American konta instrument company. And the N_2 ad-desorption isotherm environment was performed at 77.35 K and 101.3 kPa.

The pore size distribution (PSD) could be derived from adsorption or desorption branch by using the Barrett–Joyner–Halenda (BJH) model:

$$\ln \frac{p}{p_0} = -\frac{2\chi V_L}{rRT} \cos\theta, \tag{1}$$

where p is the equilibrium vapor pressure of the liquid, p_0 is the equilibrium pressure of the liquid, γ is the surface tension of the liquid, V_L is the molar volume of the liquid, θ is the contact angle, R is the gas constant, and T is the absolute temperature.

The specific surface area (SBET) is obtained by Brunauer–Emmett–Telle (BET) model:

$$\begin{cases} \dfrac{p}{V(p_0 - p)} = \dfrac{1}{V_m - c} - \dfrac{c-1}{V_m c}\dfrac{p}{p_0} \\ S_{BET} = \dfrac{V_m n_a a_m}{m V_L} \end{cases}, \tag{2}$$

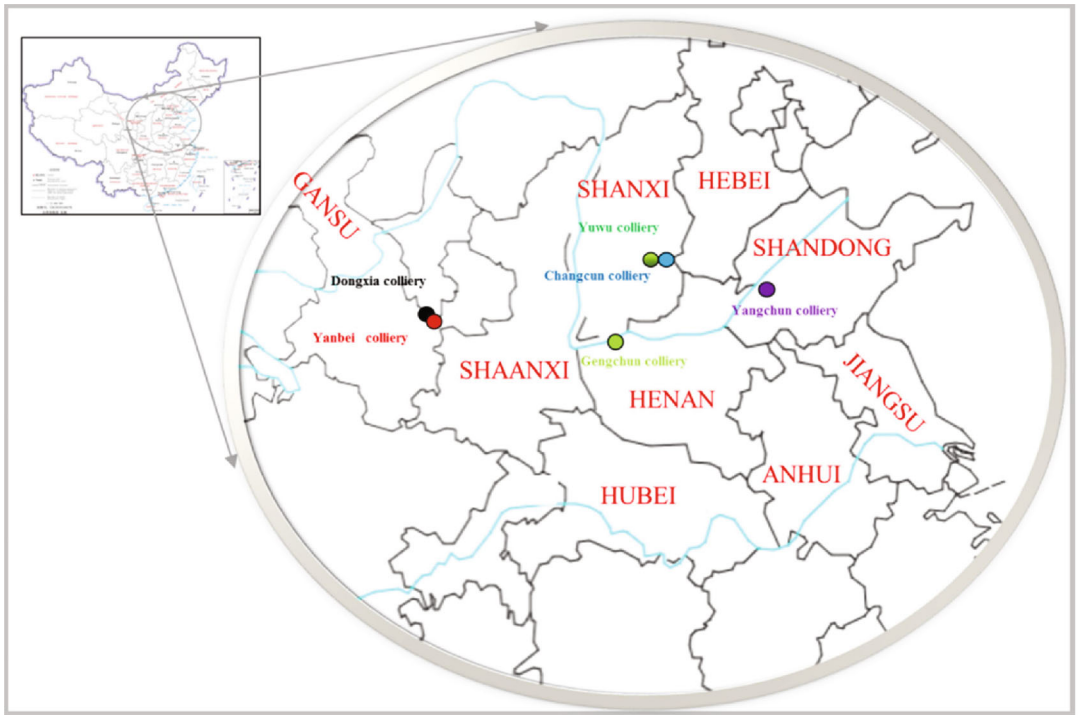

Figure 1: The location of coal samples.

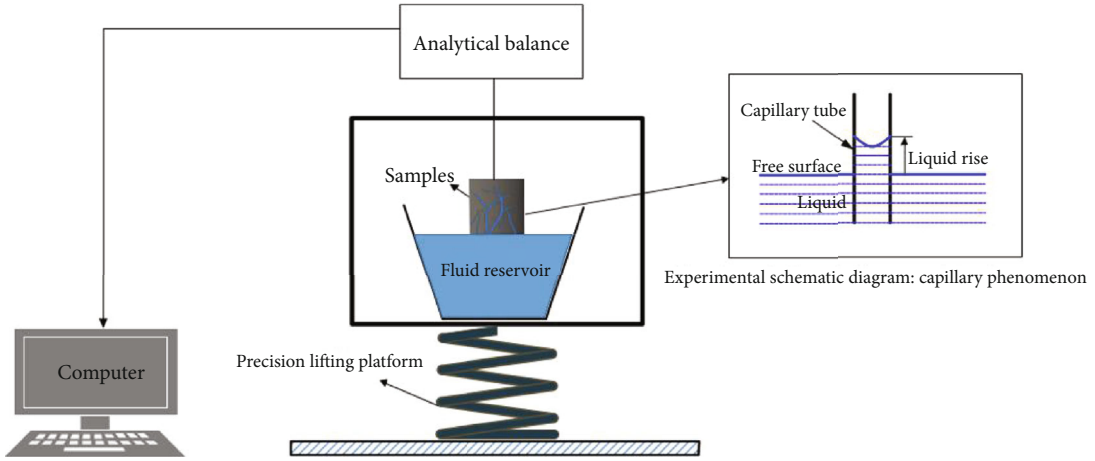

Figure 2: Schematic diagram for water imbibition experiments.

where V is volume adsorbed, V_m is the volume of the monolayer, c is the BET constant, n_a is the Avogadro constant, a_m is the cross sectional area occupied by each nitrogen molecule, and m is the sample weight.

2.2.2. Spontaneous Water Imbibition. The water imbibition test involves exposing one face of a coal sample to deionized water and measuring the mass of water uptake over time. Coal samples from the above six collieries were cut into 1 cm-sized cubes. In order to minimize fluid adsorption and evaporation, all sides except the bottom and top were coated with fast-setting epoxy. The schematic diagram for water imbibition experiments is shown in Figure 2. Prior to the imbibition test, each coal sample was oven dried at 60°C for at least 48 h. The mass variation of samples was automatically over time using a computer.

Combining the L-W regime and inertial, the most widely used analytical solution for the liquid rise in capillaries can be described by Newton's second law of motion as [22, 23]:

$$\underbrace{2\pi R\sigma\cos\theta}_{\text{surface tension}} - \underbrace{\pi R^2 y\rho g}_{\text{gravity}} - \underbrace{8\pi\mu y\frac{dy}{dt}}_{\text{viscosity}} = \underbrace{\rho\pi R^2 y\frac{d^2y}{dt^2}}_{\text{inertia forces}}, \quad (3)$$

where ρ is the density, R is the capillary radius, μ is the viscosity, σ is the surface tension, θ is the wetting angle of the liquid, t is the time, y is the height of the capillary rise, and

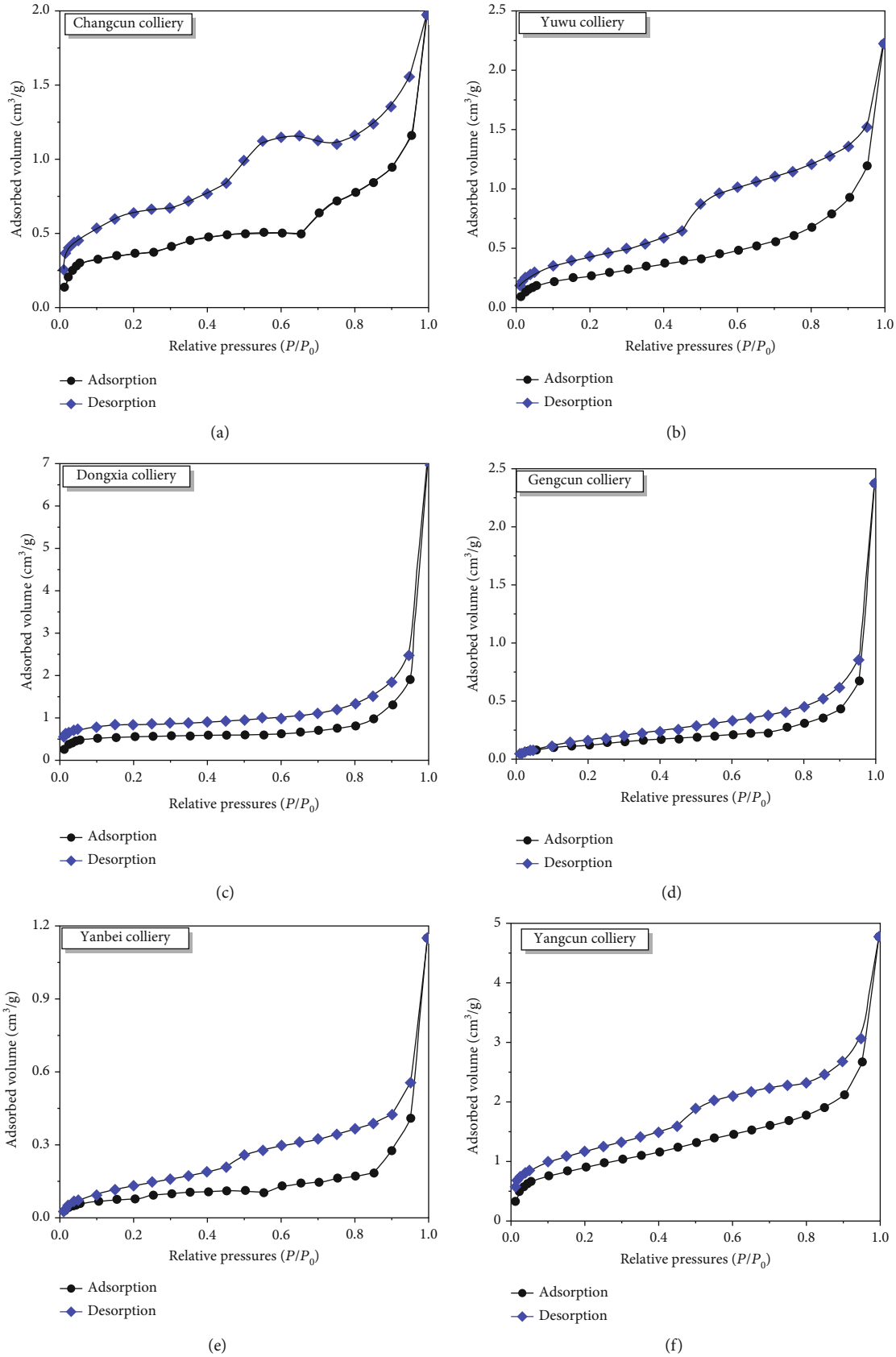

Figure 3: The isotherm curves of N_2 ad/desorption.

Table 1: Pore parameters of six coal samples measured by N_2 adsorption.

Types of coal	Total specific surface area (m^2/g)	Total pore volume (mm^3/g)	Average pore diameter (nm)	Pore volume (mm3/g)			Pore volume ratio (%)		
				<10	10-100	>100	<10	10-100	>100
Changcun	1.327	3.056	7.07	1.77	0.65	0.636	57.9	21.3	20.8
Yuwu	1.266	3.441	13.92	1.86	0.89	0.691	54.1	26.1	19.8
Dongxia	2.831	10.94	17.81	2.02	4.10	4.82	18.5	37.5	44.0
Gengcun	0.464	3.671	31.63	0.71	1.78	1.181	19.3	48.5	32.2
Yanbei	0.302	1.782	23.58	0.54	0.64	0.602	30.3	35.9	33.8
Yangcun	3.275	7.386	9.02	3.49	1.17	2.726	47.3	15.8	36.9

g is the acceleration of gravity. The capillary liquid will rise to a stationary level, h, established by the balance of gravity and capillarity,

$$h = \frac{2\sigma cos\theta}{\rho g R}. \tag{4}$$

Eq. (3) can be simplified and rewritten as

$$h - y - \frac{8\mu y}{\rho g R^2}\frac{dy}{dt} = \frac{y}{g}\frac{d^2y}{dt^2}. \tag{5}$$

Neglecting the gravity term, the transient linear momentum in Eq. (5), Lucas–Washburn equation can be derived to describe the flux rate momentum [31, 32].

$$h - y - \frac{8\mu y}{\rho g R^2}\frac{dy}{dt} = 0. \tag{6}$$

Explicit solutions by Zhmud et al. [33] corresponding to the short-time $(t \longrightarrow 0)$ and long-time limit $(t \longrightarrow \infty)$ are, respectively, expressed as

$$y = St^{0.5}\ (t \longrightarrow 0), \tag{7}$$

$$y = h\left(1 - e^{\gamma t}\right) \quad (t \longrightarrow \infty), \tag{8}$$

where $S = (R\sigma\ \cos\theta/2\mu)^{0.5}$, $\gamma = -\rho g R^2/8\mu h$. γ is the relaxation rate constant.

A detailed derivation of Eqs. (7) and (8) can be found in Zhmud et al. [33], which will be not going to go through again.

3. Results and Discuss

3.1. Pore Structure Characteristics from N_2 Adsorption Tests. N_2 adsorption isotherm curves of six samples can be found in Figure 3. It can be seen that all N_2 adsorption isotherms exhibit the similar characteristics. The hysteresis phenomenon between adsorption and desorption curves can be observed for all the samples, which is probably caused by the capillary condensation in mesoporous structures [34]. According to the International Union of Pure and Applied Chemistry (IUPAC) [35], the shapes of hysteresis loops for all the low permeability coals belong to type IV, indicating the pores are mostly in wedge-like shapes.

The pore size distributions of six coal samples derived from N_2 adsorption branch via the Barrett-Joyner-Halenda (BJH) model are presented in Figure 3. The specific surface area is obtained using the Brunauer-Emmett-Teller (BET) model [36, 37]. Pores can be classified into micropore (<10 nm), mesopore (10–100 nm), and macropore (>100 nm). Table 1 shows the statistical table of pore parameters measured by low-temperature N_2 in six coal samples. It can be seen from Figure 4 and Table 1 that the total specific surface area and total pore volume of the six coal samples are significantly different. The variation range of the total specific surface area is the range from 0.302 to 3.275 m^2/g, and the variation range of the total pore volume is the range from 1.782 to 10.94 mm^3/g. The pore structure of Changcun coal is characterized by the development of micropore. The micropore size of Changcun coal is 67.0%, and the micropore volume is 0.40mm^3/g. The pore size distribution of Yuwu coal is mainly micropore. A diameter less than 10 nm accounts for 54.1% of the total pore volume. The pore size distribution of Dongxia coal is mainly meso- and macropores, in which their total pore volume is 4.82 mm^3/g, and their pore volume accounts for 44.0% of the total pore volume, while the micropore volume only accounts for 18.5% with the micropore volume of 2.02 mm^3/g. In the pore distribution of Gengcun coal, the transitional pores, meso-, and macropores are well developed, the pore volume of the transitional pores is significantly higher than that of the micropore, accounting for 48.5% of the total pore volume, while the micropore only accounts for 19.3%. The pore distribution of Yanbei coal is uniform. The micropores, transitional pores, and macropores are well developed. The pores of Yangcun coal are mainly micropores, accounting for 47.3% with a micropore volume of 3.49mm^3/g. To sum up, the pore size distribution of coal is mainly micropores in Changcun, Yuwu, and Yangcun coals, meso- and macropores in Dongxia coal, and transitional pores in Gengcun coal. However, three type pores of transitional pores, meso-, and macropores in Yanbei coal are uniformly developed. The pore volume size from the large to small is Dongxia>Yangcun> Gengcun>Yuwu>Changcun>Yanbei coal, and the specific surface area from the large to small is Yangcun>Dongxia> Changcun>Yuwu>Gengcun>Yanbei coal.

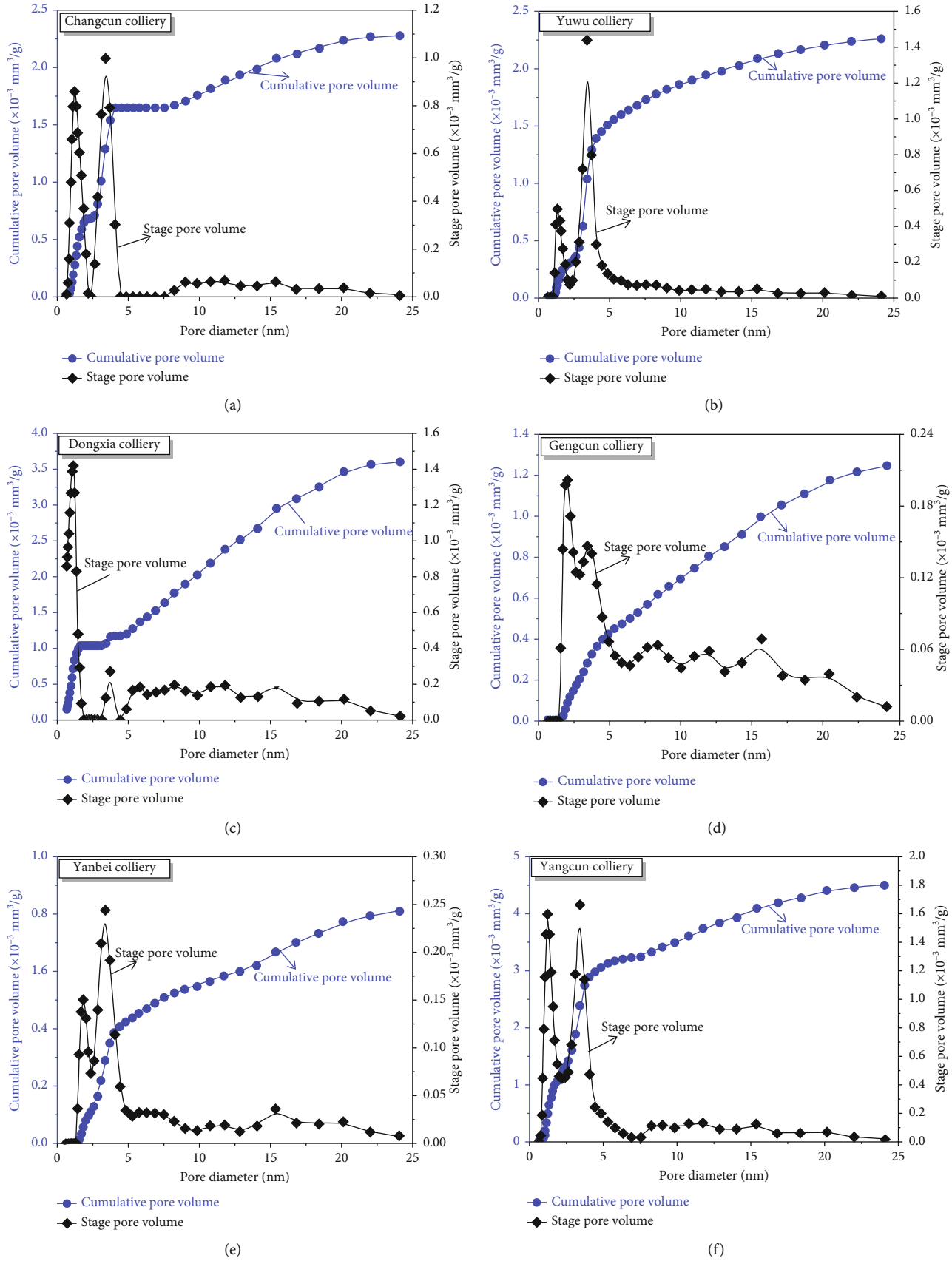

FIGURE 4: Distribution of pore volume and cumulative pore volume of coal samples at N_2 adsorption.

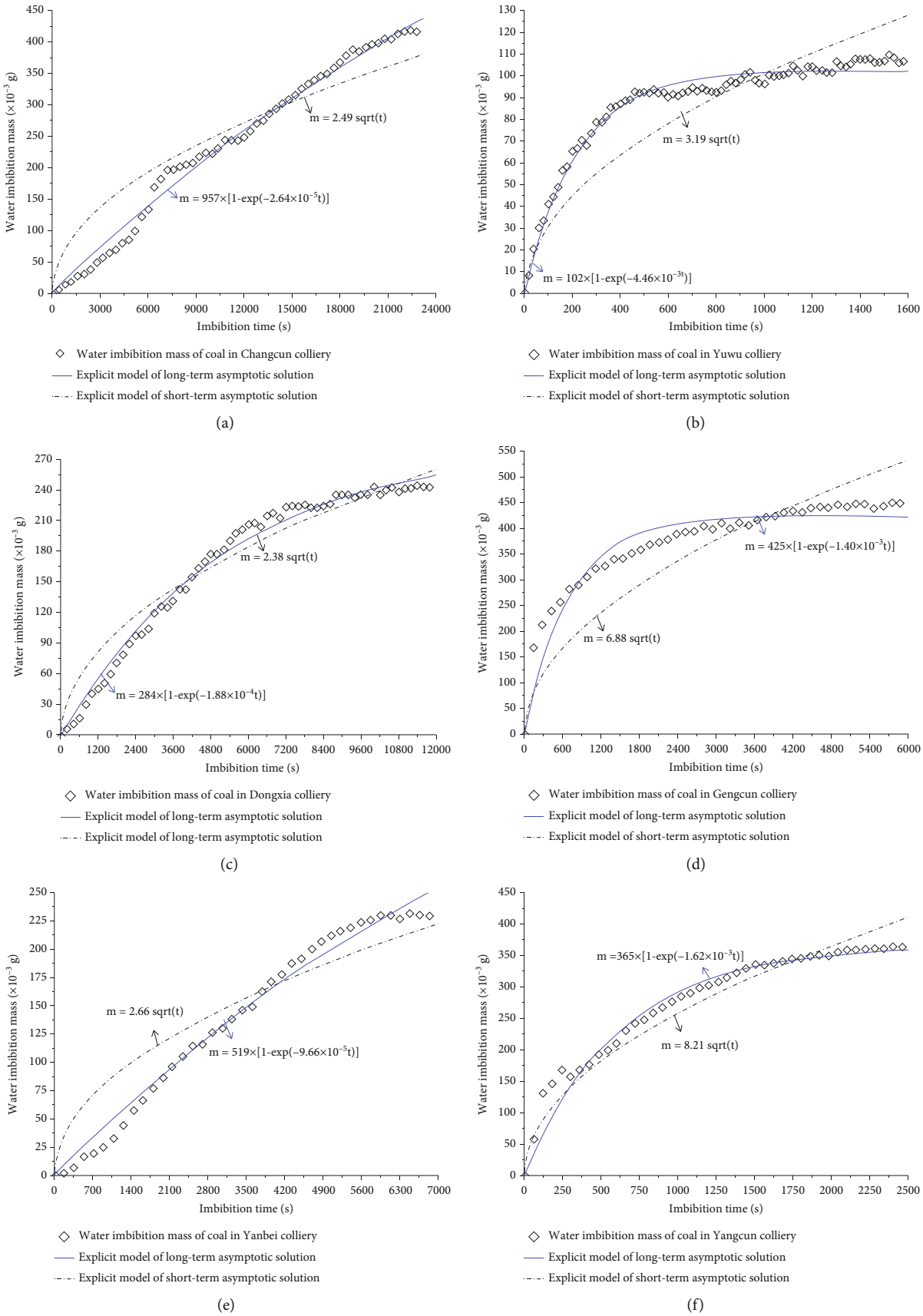

Figure 5: Evolution of water imbibition with time and the matching results of models.

Table 2: Water imbibition characteristics of six coal samples.

Types of coal	Saturated imbibition (mg)	Imbibition attenuation rate (s-1)	Relative saturated imbibition (mg/g)	Initial imbibition rate (mg/s)	Saturation time (s)	Equivalent imbibition radius reff (nm)
Changcun	957	-2.64×10^{-5}	587	0.0253	21774	182
Yuwu	102	-4.46×10^{-3}	76	0.455	1008	771
Dongxia	284	-1.88×10^{-4}	200	0.0534	10334	264
Gengcun	425	-1.40×10^{-3}	255	0.595	4467	882
Yanbei	518	-9.66×10^{-5}	334	0.0501	6159	258
Yangcun	365	-1.66×10^{-3}	210	0.591	2095	89

3.2. Capillary Imbibition of Water. By rewriting Eqs. (7) and (8), the models of coal water imbibition mass corresponding to the short-time $(t \longrightarrow 0)$ and long-time limit $(t \longrightarrow \infty)$ are, respectively, expressed as

$$m = A\rho S t^{0.5} \ (t \longrightarrow 0), \tag{9}$$

and

$$m = A\rho h\left(1 - e^{\gamma t}\right) (t \longrightarrow \infty), \tag{10}$$

where A is the cross-sectional area of the coal sample.

Figure 5 shows the evolution of the water imbibition mass of six coal samples with time and the matching results using the two models of water imbibition mass. Through the comparative analysis of Figures 5(a)–5(f), it can clearly be found that the explicit long-time limit $(t \longrightarrow \infty)$ model has a better matching effect than the explicit short-time $(t \longrightarrow 0)$ limit model. Table 2 shows the characteristic parameters of saturated imbibition mass, imbibition attenuation rate, saturated imbibition rate, initial imbibition rate, and equivalent capillary imbibition radius of six coal samples. The water imbibition mass of the coal sample is related to the water imbibition characteristics. The larger the saturated imbibition mass of the coal sample is, the stronger the capillary imbibition characteristics of the coal sample is. As shown in Figure 5 and Table 2, the relatively saturated imbibition of coal in Changcun colliery is the highest (587 mg/g), and that of Yuwu colliery is the smallest (76 mg/g). The order of saturated imbibition in six collieries from the big to small is Changcun>Yanbei>Gengcun>Yangcun>Dongxia>Yuwu colliery. Based on the pore characteristics obtained by N_2 adsorption, it can be seen that the micropores of coal are all developed from Changcun, Yuwu, and Yangcun collieries, and their micropore ratio from the high to low is Changcun >Yuwu>Yangcun colliery. The more the capillary microfissures are developed, the stronger the water imbibition capacity is. The pore size distribution of Changcun coal is similar to that of Yuwu coal, but the water imbibition capacity is quite different. It indicates that the pore connectivity of Changcun coal is better. The water imbibition capacity of Yuwu coal is weaker than that of Yangcun coal. The main reason is that the high development of pores and cracks and the high porosity of Yangcun coal. For example, the specific surface area and the pore volume of Yangcun coal are 2.96 and 2.15 times that of Yuwu coal. However, the water imbibition capacity of Yangcun coal is weaker than that of the Changcun coal, mainly because of the high ratio of the micro- and mesopores of Changcun coal. A comprehensive comparison can be considered that Changcun coal has the best connection. Similarly, among the total pore volume ratio of the micro- and mesopores of Yanbei, Gengcun, and the Dongxia coals, Yanbei coal is the largest, and Dongxia coal is the smallest. However, Dongxia coal has the higher development degree of fracture, Gengcun mine follows, and Yanbei coal is the smallest. Based on saturated water imbibition, the order of effectively connected porosity of the three coal can be obtained as Yanbei>Gengcun>Dongxia coals. Similarly, it can be seen from Table 2 that the size of meso- and macropores of Changcun coal is a close match with Yanbei coal, but the micropore distribution of Yanbei coal is smaller. So the saturated water imbibition of Changcun coal is higher than that of Yanbei coal. In Dongxia coal, micro- and macropores occupy a large proportion.

Although the pores of Dongxia coal are developed, the total pore volume and specific surface area are higher, but the connectivity may be poor, causing the saturated water imbibition of Dongxia coal to be between Yangcun and Chen coals. The development degree of pores and fissures of Gengcun coal is obviously lower than that of Yangcun coal, but the saturated water imbibition of Gengcun coal is larger. It indicates that the connected porosity of Gengcun coal is large. To sum up, the order of the effective pore connectivity of six coals is arranged from the high to the low is positively correlated with the saturated water imbibition capacity.

4. Conclusions

In this work, N_2 sorption isotherm and spontaneous imbibition tests were applied to study pore connectivity of coal and to further understand the gas migration and accumulation mechanism of these low permeability reservoirs of coal. Applied two capillary water rise models to match the imbibition data, we found the explicit long-time limit $(t \longrightarrow \infty)$ is better than the short-time limit $(t \longrightarrow 0)$, because of considering the more important factors. In addition, combining N_2 sorption isotherm with spontaneous imbibition test analysis, it is found that the effective pore connectivity of coal is positively correlated with its relative saturation imbibition of

coal. Unfortunately, the parameters including the Ro, proximate analysis parameters, and macerals are not in-depth discussion and analysis in this work. In the later stage, the influences of the above parameters on pore structure and permeability can be further considered.

Data Availability

The data used to support the findings of this study are available from the corresponding author upon request.

Conflicts of Interest

The authors declare that they have no conflicts of interest.

Acknowledgments

This work was supported by the National Science Foundation of China (52074284), China's state key research and Development Program (2018YFC0808100), Open Fund of Shaanxi Key Laboratory of Geological Support for Coal Green Exploitation (DZBZ2020-09), and State Key Laboratory of Coal Resources in Western China (SKLCRKF20-12).

References

[1] C. Ö. Karacan, F. A. Ruiz, M. Cotè, and S. Phipps, "Coal mine methane: a review of capture and utilization practices with benefits to mining safety and to greenhouse gas reduction," *International Journal of Coal Geology*, vol. 86, no. 2-3, pp. 121–156, 2011.

[2] S. Tao, Z. J. Pan, S. D. Chen, and S. L. Tang, "Coal seam porosity and fracture heterogeneity of marcolithotypes in the Fanzhuang Block, southern Qinshui Basin, China," *Journal of Natural Gas Science and Engineering*, vol. 66, pp. 148–158, 2019.

[3] S. Tao, S. D. Chen, D. Z. Tang, X. Zhao, H. Xu, and S. Li, "Material composition, pore structure and adsorption capacity of low-rank coals around the first coalification jump: A case of eastern Junggar Basin, China," *Fuel*, vol. 211, pp. 804–815, 2018.

[4] X. Men, S. Tao, Z. X. Liu, W. Tian, and S. Chen, "Experimental study on gas mass transfer process in a heterogeneous coal reservoir," *Fuel Processing Technology*, vol. 216, 2021.

[5] X. B. Zhang and Q. H. Hu, "Development of geothermal resources in China: a review," *Journal of Earth Science*, vol. 29, no. 2, pp. 452–467, 2018.

[6] S. Lu, J. Li, P. Zhang et al., "Classification of microscopic pore-throats and the grading evaluation on shale oil reservoirs," *Petroleum Exploration and Development*, vol. 45, no. 3, pp. 452–460, 2018.

[7] M. A. Q. Siddiqui, S. Ali, H. Fei, and H. Roshan, "Current understanding of shale wettability: a review on contact angle measurements," *Earth Science Reviews*, vol. 181, pp. 1–11, 2018.

[8] M. D. Sun, B. S. Yu, Q. H. Hu, R. Yang, Y. Zhang, and B. Li, "Pore connectivity and tracer migration of typical shales in south China," *Fuel*, vol. 203, pp. 32–46, 2017.

[9] Q. H. Hu, R. P. Ewing, and S. Dultz, "Low pore connectivity in natural rock," *Journal of Contaminant Hydrology*, vol. 133, pp. 76–83, 2012.

[10] X. B. Yuan, Y. B. Yao, D. M. Liu, and Z. Pan, "Spontaneous imbibition in coal: experimental and model analysis," *Journal of Natural Gas Science and Engineering*, vol. 67, pp. 108–121, 2019.

[11] G. L. Sheng, Y. Su, F. Javadpour et al., "New slip coefficient model considering adsorbed gas diffusion in shale gas reservoirs," *Energy & Fuels*, vol. 34, no. 10, pp. 12078–12087, 2020.

[12] S. F. Zhang and J. Sheng, "Effect of water imbibition on hydration induced fracture and permeability of shale cores," *Journal of Natural Gas Science and Engineering*, vol. 45, pp. 726–737, 2017.

[13] H. Bahrami, R. Rezaee, and B. Clennell, "Water blocking damage in hydraulically fractured tight sand gas reservoirs: an example from Perth Basin, Western Australia," *Journal of Petroleum Science and Engineering*, vol. 88-89, pp. 100–106, 2012.

[14] Y. Cheng, "Impact of water dynamics in fractures on the performance of hydraulically fractured wells in gas-shale reservoirs," *Journal of Canadian Petroleum Technology*, vol. 51, no. 2, pp. 143–151, 2012.

[15] H. Singh, "A critical review of water uptake by shales," *Journal of Natural Gas Science and Engineering*, vol. 34, pp. 751–766, 2016.

[16] H. Dehghanpour, H. A. Zubair, A. Chhabra, and A. Ullah, "Liquid intake of organic shales," *Energy & Fuels*, vol. 26, no. 9, pp. 5750–5758, 2012.

[17] W. Heber Green and G. A. Ampt, "Studies on soil Phyics," *Journal of Agriculture Science (Cambridge)*, vol. 4, no. 1, pp. 1–24, 1911.

[18] R. Lucas, "Ueber das Zeitgesetz des kapillaren Aufstiegs von Flüssigkeiten," *Kolloid Zeitschrift*, vol. 23, no. 1, pp. 15–22, 1918.

[19] E. W. Washburn, "The dynamics of capillary flow," *Physics Review*, vol. 17, no. 3, pp. 273–283, 1921.

[20] R. Masoodi, E. Languri, and A. Ostadhossein, "Dynamics of liquid rise in a vertical capillary tube," *Journal of Colloid and Interface Science*, vol. 389, no. 1, pp. 268–272, 2013.

[21] N. Fries and M. Dreyer, "An analytic solution of capillary rise restrained by gravity," *Journal of Colloid and Interface Science*, vol. 320, no. 1, pp. 259–263, 2008.

[22] O. H. Mohammad and A. A. Bassam, "Modeling meniscus rise in capillary tubes using fluid in rigid-body motion approach," *Communications in Nonlinear Science and Numerical Simulation*, vol. 57, pp. 449–460, 2018.

[23] B. Roychaudhuri, T. T. Tsotsis, and K. Jessen, "An experimental investigation of spontaneous imbibition in gas shales," *Journal of Petroleum Science and Engineering*, vol. 111, pp. 87–97, 2013.

[24] H. Dehghanpour, Q. Lan, Y. Saeed, H. Fei, and Z. Qi, "Spontaneous imbibition of brine and oil in gas shales: effect of water adsorption and resulting microfractures," *Energy & Fuels*, vol. 27, no. 6, pp. 3039–3049, 2013.

[25] Z. Gao and Q. Hu, "Wettability of Mississippian Barnett Shale samples at different depths: investigations from directional spontaneous imbibition," *AAPG Bulletin*, vol. 100, no. 1, pp. 101–114, 2016.

[26] Z. Gao and Q. Hu, "Initial water saturation and imbibition fluid affect spontaneous imbibition into Barnett shale samples," *Journal of Natural Gas Science and Engineering*, vol. 34, pp. 541–551, 2016.

[27] J. Wu, Z. Wang, W. Su, and J. Chen, "Comprehensive influence of self-adsorbed water on gas desorption in coal," *Coal geology & exploration*, vol. 45, pp. 35–40, 2017.

[28] J. C. Cai, X. Y. Hu, D. C. Standnes, and L. You, "An analytical model for spontaneous imbibition in fractal porous media including gravity," *Colloids and Surfaces A: Physicochemical and Engineering Aspects*, vol. 414, pp. 228–233, 2012.

[29] A. A. Hinai, R. Rezaee, L. Esteban, and M. Labani, "Comparisons of pore size distribution: a case from the Western Australian gas shale formations," *Journal of Unconventional Oil and Gas Resources*, vol. 8, pp. 1–13, 2014.

[30] G. L. Sheng, H. Zhao, Y. L. Su et al., "An analytical model to couple gas storage and transport capacity in organic matter with noncircular pores," *Fuel*, vol. 268, p. 117288, 2020.

[31] J. R. Ligenza and R. B. Bernstein, "The rate of rise of liquids in fine vertical capillaries," *Journal of the American Chemical Society*, vol. 73, no. 10, pp. 4636–4638, 1951.

[32] A. Hamraoui and T. Nylander, "Analytical approach for the Lucas-Washburn equation," *Journal of Colloid and Interface Science*, vol. 250, no. 2, pp. 415–421, 2002.

[33] B. Zhmud, F. Tiberg, and K. Hallstensson, "Dynamics of capillary rise," *Journal of Colloid and Interface Science*, vol. 228, no. 2, pp. 263–269, 2000.

[34] P. A. Monson, "Understanding adsorption/desorption hysteresis for fluids in mesoporous materials using simple molecular models and classical density functional theory," *Microporous and Mesoporous Materials*, vol. 160, pp. 47–66, 2012.

[35] P. Zhao, X. Wang, J. Cai et al., "Multifractal analysis of pore structure of Middle Bakken formation using low temperature N_2 adsorption and NMR measurements," *Journal of Petroleum Science and Engineering*, vol. 176, pp. 312–320, 2019.

[36] Z. Xi, S. Tang, J. Wang, G. Yang, and L. Li, "Formation and development of pore structure in marine-continental transitional shale from northern China across a maturation gradient: insights from gas adsorption and mercury intrusion," *International Journal of Coal Geology*, vol. 200, pp. 87–102, 2018.

[37] X. Zheng, B. Zhang, H. Sanei et al., "Pore structure characteristics and its effect on shale gas adsorption and desorption behavior," *Marine and Petroleum Geology*, vol. 100, pp. 165–178, 2019.